Novel Gallium Phosphate Framework Encapsulating Trinuclear $Mn_3(H_2O)_6O_8$ Cluster: Hydrothermal Synthesis and Characterization of $Mn_3(H_2O)_6Ga_4(PO_4)_6$

Kuei-Fang Hsu and Sue-Lein Wang*

Department of Chemistry, National Tsing Hua University, Hsinchu, Taiwan 300

Received November 18, 1999

A new manganese gallium phosphate, $Mn_3(H_2O)_6Ga_4(PO_4)_6$, has been synthesized under hydrothermal conditions at 150 °C and characterized by single-crystal X-ray diffraction, thermogravimetric analysis, magnetic susceptibility, and electron paramagnetic resonance (EPR) spectroscopy. It crystallized in the monoclinic space group, $P2_1/n$, with $a = 8.9468(4)$ Å, $b = 10.1481(5)$ Å, $c = 13.5540(7)$ Å, $\beta = 108.249(1)°$, and $Z = 2$. The compound is unusual in that it is not only the first nonorganically templated MnGaPO phase but also the first instance where edge-shared trinuclear manganese−oxygen clusters are encapsulated in a metal phosphate lattice. The trimer involves a central $Mn(H_2O)_4O_2$ octahedron, which links to two Mn $(H_2O)_2O_4$ octahedra at trans edges. The $Mn_3(H_2O)_6O_8$ clusters reside in tunnels built from GaO_5 trigonal bipyramids and PO_4 tetrahedra. Our magnetic study revealed that superexchange interactions occurred between the neighboring Mn^{II} centers. A good fit of the magnetic susceptibility data for the isolated trimers was obtained by using a derived expression based on Van Vleck's equation. Unlike all existing linear trinuclear Mn^{II} complexes, the $\chi_M T$ product in the range 8−4 K remains at a constant value corresponding to one spin $S = {}^5/_2$ per three Mn^{II} centers. The Curie behavior at such low temperatures has been confirmed by EPR data. According to the thermogravimetric analysis/differential thermal analysis (TGA/DTA) results, the title compound is thermally stable up to ca. 200 °C.

Introduction

The partial replacement of Al^{3+} by M^{2+} (M = first-row transition metals) in the frameworks of aluminum phosphates is well-known for their rich structural chemistry and interesting catalytic properties,[1] exemplified by MnAlPO-31 for the isomerization of 1-butene,[2] and MnAlPO-5, which demonstrates reversible cycles of oxidation and reduction.[3] The search for gallium phosphates that adopt microporous frameworks has attracted much interest since the report of the first compound, $(Pr^iNH_3)[Ga_4(PO_4)_4(OH)]\cdot H_2O$,[4] with a structure similar to those of the $AlPO_4$ family. Cloverite[5] is another example, which is a much noted gallium phosphate for its unique microporous framework, containing 29−30 Å supercages. In contrast to the aluminum phosphates, a limited number of MGaPO compounds (M = Mn^{2+}, Fe^{2+}, Co^{2+}, Zn^{2+})[6−14] were synthesized. To date, only three Mn-substituted gallium phosphates were previously documented by others. The first, MnGaPO-1,[9] adopts the laumontite structure in which Mn^{2+} and Ga^{3+} ions are disordered at the same tetrahedral sites; the second, MnGaPO-2,[10] adopts a unique open framework where Mn^{2+} and Ga^{3+} ions occupy two distinct sites in five- and four-coordination, respectively. The third[14] is isotypic with $NH_4[CoGa_2(PO_4)_3(H_2O)_2]$[8] where Mn^{2+} ions are in distorted octahedral sites.

We have been interested in the synthesis of novel open-frameworks of transition metal phosphates and arsenates by incorporating both inorganic and organic cations as structure-directing reagents.[15] Because not many manganese-substituted gallium phosphates are known, we thought of exploring the possibility of synthesizing new phases in the system. Our efforts have resulted in the preparation of an organically templated mixed-valence compound, $(pipz)_2Mn_2Ga_5(H_2O)(PO_4)_8$,[16] and an unusual Mn^{II} species, $Mn_3(H_2O)_6Ga_4(PO_4)_6$ (**1**). Compound **1** is the first MGaPO phase where clusters of Mn−O polyhdra are in place of organic templates. The encapsuled trinuclear $Mn_3(H_2O)_6O_8$ cluster in such a GaPO framework results in very interesting magnetic behavior. Herein, the hydrothermal synthesis, crystal structure, thermal analysis, and magnetic study of **1** are presented.

Experimental Section

Synthesis and Compositional Characterization. Chemicals of reagent grade were used as received. A mixture of 4,4′-trimethylenedipiperidine (0.631 g, 3 mmol), $Ga(NO_3)_3\cdot xH_2O$ (0.384 g, 1.5 mmol),

(1) Hartmann, M.; Kevan, L. *Chem. Rev.* **1999**, *99*, 635.
(2) Zubowa, H. L.; Richter, M.; Roost, U.; Parlitz, B.; Fricke, R. *Catal. Lett.* **1993**, *19*, 67.
(3) Katzmarzyk, A.; Ernst, S.; Weitkamp, J.; Knozinger, H. *Catal. Lett.* **1991**, *9*, 85.
(4) Parise, J. B. *J. Chem. Soc., Chem. Commun.* **1985**, 606.
(5) Estermann, M.; McCusker, L. B.; Baerlocher, C.; Merrouche, A.; Kessler, H. *Nature* **1991**, *352*, 320.
(6) Chippindale, A. M.; Walton, R. I. *J. Chem. Soc., Chem. Commun.* **1994**, 2453.
(7) Cowley, A. R.; Chippindale, A. M. *Chem. Commun.* **1996**, 673.
(8) Chippindale, A. M.; Cowley, A. R.; Walton, R. I. *J. Mater. Chem.* **1996**, *6*, 611.
(9) Bond, A. D.; Chippindale, A. M.; Cowley, A. R. *Zeolites* **1997**, *19*, 326.
(10) Chippindale, A. M.; Bond, A. D.; Cowley, A. R. *Chem. Mater.* **1997**, *9*, 2830.
(11) Chippindale, A. M.; Cowley, A. R. *Zeolites* **1997**, *18*, 176.
(12) Chippindale, A. M.; Cowley, A. R.; Peacock, K. J. *Microporous Mesoporous Mater.* **1998**, *24*, 133.
(13) Cowley, A. R.; Chippindale, A. M. *Microporous Mesoporous Mater.* **1999**, *28*, 163.
(14) (a) Chippindale, A. M.; Cowley, A. R.; Bond, A. D. *Acta Crystallogr., Sect. C* **1998**, *54*, 1. (b) Overweg, A. R.; de Haan, J. W.; Magusin, P. C. M. M.; van Santen, R. A.; Sankar, G.; Thomas, J. M. *Chem. Mater.* **1999**, *11*, 1680.
(15) (a) Hsu, K. F.; Wang, S. L. *Chem. Mater.* **1999**, *11*, 1876. (b) Tsai, Y. M.; Wang, S. L.; Huang, C. H.; Lii, K. H. *Inorg. Chem.* **1999**, *38*, 4183. (c) Hsu, K. F.; Wang, S. L. *Inorg. Chem.* **1998**, *37*, 3230. (d) Chang, R. S.; Wang, S. L.; Lii, K. H. *Inorg. Chem.* **1997**, *36*, 3410. (e) Fan, N. Y.; Wang, S. L. *Inorg. Chem.* **1996**, *35*, 4708.
(16) Hsu, K. F.; Wang, S. L. *Chem. Commun.* **2000**, 135.

10.1021/ic991340s CCC: $19.00
Published on Web 03/17/2000

Table 1. Crystallographic Data for **1**

chemical formula	$H_{12}Ga_4Mn_3O_{30}P_6$
fw	1121.6
space group	$P2_1/n$
a, Å	8.9468(4)
b, Å	10.1481(5)
c, Å	13.5540(7)
β, deg	108.249(1)
V, Å^3	1168.7(1)
Z	4
ρ_{calc}, g cm^{-3}	3.187
μ, mm^{-1}	6.657
T, °C	23
λ, Å	0.710 73
$R(F_o)^a$	0.0364
$R_w(F_o^2)^b$	0.0949

^{a} $R(F_o) = \sum||F_o| - |F_c||/\sum|F_o|$. ^{b} $R_w(F_o^2) = [\sum[w(F_o^2 - F_c^2)]^2/\sum[w(F_o^2)^2]]^{1/2}$, $w = [\sigma_2(F_o) + (0.0578P)^2 + 4.4516P]^{-1}$, where $P = (F_o^2 + 2F_c^2)/3$.

Table 2. Atomic Coordinates and Thermal Parameters (Å^2) for **1**

atom	x	y	z	$U_{eq}{}^a$
Ga(1)	0.4311(1)	0.0807(1)	−0.1679(1)	0.005(1)
Ga(2)	0.0700(1)	0.0662(1)	0.1702(1)	0.005(1)
Mn(1)	0.2766(1)	0.2800(1)	0.0079(1)	0.013(1)
Mn(2)	0.0	0.5	0.0	0.027(1)
P(1)	0.3274(2)	0.3803(2)	−0.2081(1)	0.007(1)
P(2)	0.1838(2)	0.3597(2)	0.2194(1)	0.006(1)
P(3)	0.2503(2)	−0.0034(2)	−0.0011(1)	0.005(1)
O(1)	0.3323(6)	0.4033(5)	−0.0965(4)	0.015(1)
O(2)	0.4537(5)	0.4645(5)	−0.2311(4)	0.009(1)
O(3)	0.3438(5)	0.2343(5)	−0.2323(4)	0.010(1)
O(4)	0.1625(5)	0.4192(5)	−0.2834(4)	0.011(1)
O(5)	0.1675(5)	0.2128(5)	0.2406(3)	0.009(1)
O(6)	0.3456(5)	0.3970(5)	0.2965(4)	0.009(1)
O(7)	0.0540(6)	0.4435(5)	0.2381(4)	0.011(1)
O(8)	0.1800(6)	0.3847(5)	0.1070(4)	0.011(1)
O(9)	0.2974(6)	0.0957(5)	−0.0730(4)	0.011(1)
O(10)	0.1996(6)	0.0902(5)	0.0724(4)	0.011(1)
O(11)	0.3869(5)	−0.0938(5)	0.0526(4)	0.009(1)
O(12)	0.1153(5)	−0.0947(5)	−0.0607(4)	0.011(1)
O(13)	0.5035(6)	0.3026(5)	0.1170(4)	0.025(1)
O(14)	0.0192(6)	0.3313(5)	−0.1084(4)	0.017(1)
O(15)	0.1971(7)	0.6179(6)	−0.0200(5)	0.034(2)

^{a} U_{eq} is defined as one-third of the trace of the orthogonalized U_{ij} tensor.

$MnCl_2 \cdot 4H_2O$ (0.297 g, 1.5 mmol), 85% H_3PO_4 (0.4 mL, 6 mmol), $C_2H_6O_2$ (5.8 mL), and H_2O (5.8 mL) was placed in a Teflon lined digestion bomb with an internal volume of 23 mL and heated at 150 °C under autogenous pressure for 3 days followed by slow cooling to 30 °C at 6 °C h^{-1}. The product was filtered off, washed with water, rinsed with ethanol, and dried in a desiccator at ambient temperature. The final product contained a small amount of colorless columnar crystals of $Mn_3(H_2O)_6Ga_4(PO_4)_6$ (**1**) (vide infra) and a relatively large amount of colorless needles of $Mn_5(H_2O)_4(HPO_4)_2(PO_4)_2$.[17]

The above reaction condition was adapted from that for the preparation of the mixed-valence compound $(pipz)_2Mn_2Ga_5(H_2O)(PO_4)_8$,[16] except a different organic amine was employed. It was noted that although the crystals of **1** contain no organic part, the presence of an amine bulkier than piperazine in the reaction mixture was essential for obtaining **1**. An optimum condition for the preparation of **1** was later achieved by reducing the quantities of Ga and Mn to 0.8 and 0.6 mmol, respectively, while keeping the others the same. The product contained columnar crystals of **1** as a major phase and a tiny amount of the known compound $Mn_5(H_2O)_4(HPO_4)_2(PO_4)_2$.[17] The atomic ratios of Mn/Ga/P determined from single-crystal structure refinements (3:4:6) for **1** were further confirmed by electron probe microanalysis (EPMA) data (3.04/4.07/6.00).

Single-Crystal X-ray Structure Analysis. A crystal of dimensions 0.10 mm × 0.03 mm × 0.03 mm for **1** was selected for indexing and intensity data collection. The measurement was performed on a Siemens Smart-CCD diffractometer system equipped with a normal focus and a 3 kW sealed-tube X-ray source (λ = 0.710 73 Å). Intensity data were collected in 1271 frames with increasing ω (width of 0.3° per frame). Unit cell dimensions were determined by a least-squares fit of 2745 reflections. The intensity data were corrected for *Lp* and absorption

(17) Gerault, Y.; Riou, A.; Cudennec, Y. *Acta Crystallogr.* **1987**, *C43*, 1829.

Table 3. Selected Bond Lengths (Å) and Bond Valence Sums ($\sum$s) for **1**

Ga(1)−O(3)	1.836(5)	Ga(1)−O(7)^c	1.941(5)
Ga(1)−O(4)^a	1.864(5)	Ga(1)−O(9)	2.019(5)
Ga(1)−O(11)^b	1.874(5)		
$\sum$s[Ga(1)−O] = 3.07			
Ga(2)−O(5)	1.833(5)	Ga(2)−O(2)^f	1.959(5)
Ga(2)−O(12)^d	1.871(5)	Ga(2)−O(10)	2.029(5)
Ga(2)−O(6)^e	1.873(5)		
$\sum$s[Ga(2)−O] = 3.12			
Mn(1)−O(1)	2.062(5)	Mn(1)−O(9)	2.204(5)
Mn(1)−O(8)	2.099(5)	Mn(1)−O(10)	2.308(5)
Mn(1)−O(13)	2.118(5)	Mn(1)−O(14)	2.403(5)
$\sum$s[Mn(1)−O] = 2.07			
Mn(2)−O(8)^g	2.146(5)	Mn(2)−O(15)^g	2.216(6)
Mn(2)−O(8)	2.146(5)	Mn(2)−O(14)^g	2.293(5)
Mn(2)−O(15)	2.216(6)	Mn(2)−O(14)	2.293(5)
$\sum$s[Mn(2)−O] = 1.90			
P(1)−O(1)	1.518(5)	P(1)−O(3)	1.536(5)
P(1)−O(2)	1.525(5)	P(1)−O(4)	1.560(5)
$\sum$s[P(1)−O] = 5.05			
P(2)−O(5)	1.534(5)	P(2)−O(7)	1.523(5)
P(2)−O(6)	1.545(5)	P(2)−O(8)	1.535(5)
$\sum$s[P(2)−O] = 5.05			
P(3)−O(9)	1.548(5)	P(3)−O(11)	1.519(5)
P(3)−O(10)	1.546(5)	P(3)−O(12)	1.536(5)
$\sum$s[P(3)−O] = 5.00			
O(13)−H(1)	0.923	O(13)−H(2)	0.947
O(14)−H(3)	0.815	O(14)−H(4)	0.881
O(15)−H(5)	1.091	O(14)−H(6)	1.284
H(1)···O(2)^h	1.864	O(13)···2)^h	2.782
H(2)···O(4)^i	2.019	O(13)···O(4)^i	2.773
O(13)−H(1)···O(2)^h	172.9°	O(13)−H(2)···O(4)^i	135.3°
H(3)···O(6)^j	2.075	O(14)···O(6)^j	2.862
H(4)···O(7)^k	2.199	O(14)···O(7)^k	2.836
O(14)−H(3)···O(6)^j	162.7°	O(13)−H(4)···O(7)^k	128.9°
H(6)···O(12)^l	1.808	O(15)···O(12)^l	3.012
O(15)−H(6)···O(12)^l	153.4°		

^{a} Symmetry code $-x + 1/2, y - 1/2, -z - 1/2$. ^{b} Symmetry code $-x + 1, -y, -z$. ^{c} Symmetry code $x + 1/2, -y + 1/2, z - 1/2$. ^{d} Symmetry code $-x, -y, -z$. ^{e} Symmetry code $-x + 1/2, y - 1/2, -z + 1/2$. ^{f} Symmetry code $x - 1/2, -y + 1/2, z + 1/2$. ^{g} Symmetry code $-x, -y + 1, -z$. ^{h} Symmetry code $-x + 1, -y + 1, -z$. ^{i} Symmetry code $x + 1/2, -y + 1/2, z + 1/2$. ^{j} Symmetry code $x - 1/2, -y + 1/2, z - 1/2$. ^{k} Symmetry code $-x, -y + 1, -z$. ^{l} Symmetry code $x, y + 1, z$.

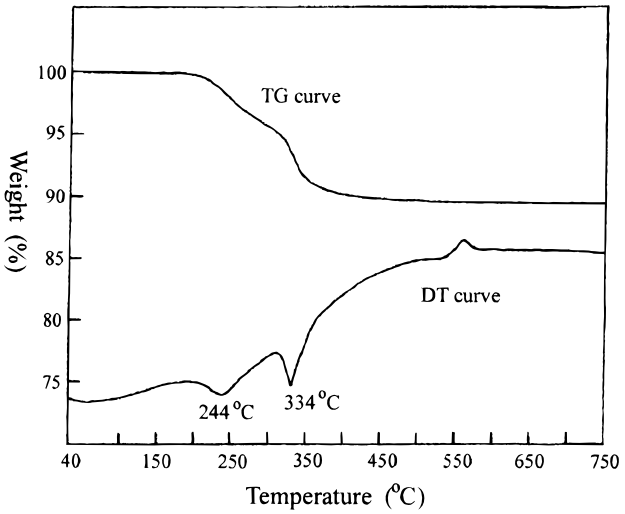

Figure 1. TGA and DTA curves of $Mn_3(H_2O)_6Ga_4(PO_4)_6$.

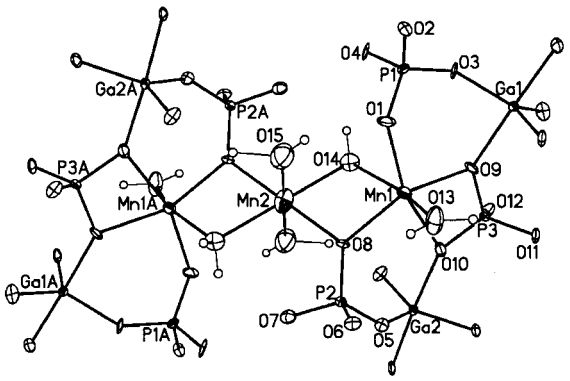

Figure 2. ORTEP drawing of the building unit in structure **1**. Thermal ellipsoids are given at the 50% level.

effects. The number of measured and observed independent reflections ($I_{obs} > 2\sigma_I$) is 1665 and 1336. Corrections for absorption effects were based on symmetry-equivalent reflections using the SADABS program.[18] On the basis of systematic absences and statistics of intensity distribution, the space group was determined to be $P2_1/n$ for **1**. Direct methods were used to locate the gallium, manganese, phosphorus, and a few oxygen atoms with the remaining atoms being found from successive difference maps. The result of bond-length and bond-strength calculations[19] was used to identify the water oxygens, O(13), O(14), and O(15). All of the hydrogen atoms were directly located from a Fourier difference map calculated at the final stage of structure refinements. The final cycle of refinement, including the atomic coordinates and anisotropic thermal parameters for all non-hydrogen atoms and fixed atomic coordinates and isotropic thermal parameters for H atoms, converged at R1 = 0.0364 and wR2 = 0.0949. Corrections for secondary extinction and anomalous dispersion were applied. Neutral-atom scattering factors for all atoms were taken from the standard sources. Calculations were performed on a PC using SHELXTL-Plus programs.[20] The crystallographic data are listed in Table 1, atomic coordinates and thermal parameters in Table 2, and selected bond lengths and bond-valence sums in Table 3.

Additional crystallographic results are given in Supporting Information.

Thermogravimetric Analysis. Thermal analysis, using a Seiko TG/DTA 300 analyzer, was performed on a powder sample of picked-up crystals of **1** (7.0 mg) under flowing N_2 with a heating rate of 10 °C min^{-1}. The title compound is thermally stable to ca. 200 °C, as indicated by the thermogravimetric analysis/differential thermal analysis (TGA/DTA) curves shown in Figure 1. The weight loss occurred in two steps: the range from 200 to ca. 285 °C corresponds to the release of two H_2O molecules (calcd, 3.21%), and the range from ca. 285 to 450 °C corresponds to the release of four H_2O molecules (calcd, 6.42%). Although the two steps did not resolve well, the total observed weight loss (10.4%) compares well with the calculated value (9.63%).

Magnetic Susceptibility and EPR Measurements. A 11.0 mg powder sample was used to collect variable temperature magnetic susceptibility $\chi(T)$ data from 2 to 300 K in a magnetic field of 0.5 T using a Quantum Design SQUID magnetometer. The measured susceptibilities have been corrected for core diamagnetism.[21] X-band electron paramagnetic resonance (EPR) spectra were recorded on a 80 mg powder sample between 4.2 and 300 K with a Brucker EMX-10 spectrometer equipped with variable temperature controllers.

Results and Discussion

The unique structure of **1** consists of $Mn(H_2O)_2O_4$ and $Mn(H_2O)_4O_2$ octahedra, GaO_5 trigonal bipyramids, and PO_4 tetrahedra. As depicted in Figure 2, the two crystallographic Mn sites, Mn(1) and Mn(2), are respectively coordinated by two and four H_2O molecules. The Mn(2) octahedron lies on an inversion center and shares trans edges with two Mn(1) octahedra, leading to the formation of the linear trinuclear $Mn_3(H_2O)_6O_8$ cluster. The trimeric unit has a topology similar to those of the molecular complexes $Mn_3(RCO_2)_6(L)_2 \cdot nH_2O$ (L = bpy, BiPhMe, phen, pybim),[22] where octahedra of MnN_2O_4 exist. In the extended structures, isolated linear Mn−O−Mn−O−Mn units were not previously documented. Triangular trimers of $Mn^{II}O_6$ octahedra were found to exist in a few

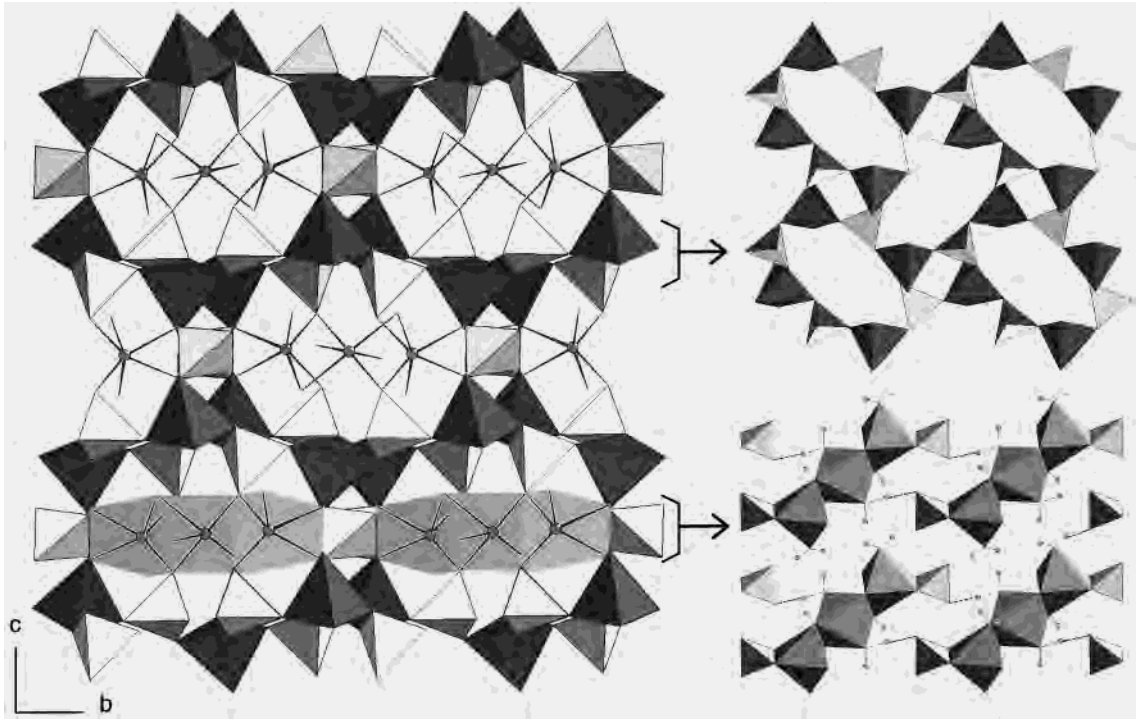

Figure 3. Polyhedral representations of $Mn_3(H_2O)_6Ga_4(PO_4)_6$. To the left is the projection of the structure showing the $Mn_3(H_2O)_6$ cores (balls for Mn centers and sticks for H_2O ligands) that reside in the tunnels built of GaO_5 trigonal bipyramids (darker polyhedra) and PO_4 tetrahedra (lighter polyhedra). At top-right is the porous $GaPO_4$ layers viewed perpendicular to the tunnel direction. At bottom-right is the Mn_3P_2 pentamers in the interlayer region. Dotted lines indicate H-bonds.

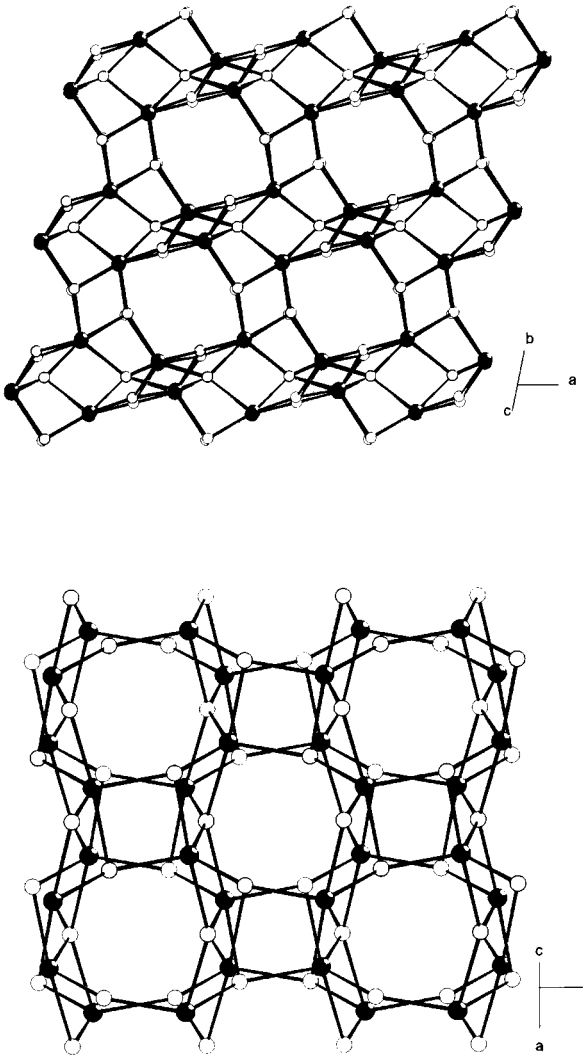

Figure 4. Anionic framework of $[Ga_3(PO_4)_6]$ in **1** showing the intersecting tunnels along [011] (top) and [101] (bottom). In these plots, only the polyhedral centers are shown, where shaded circles are for Ga and open circles are for P.

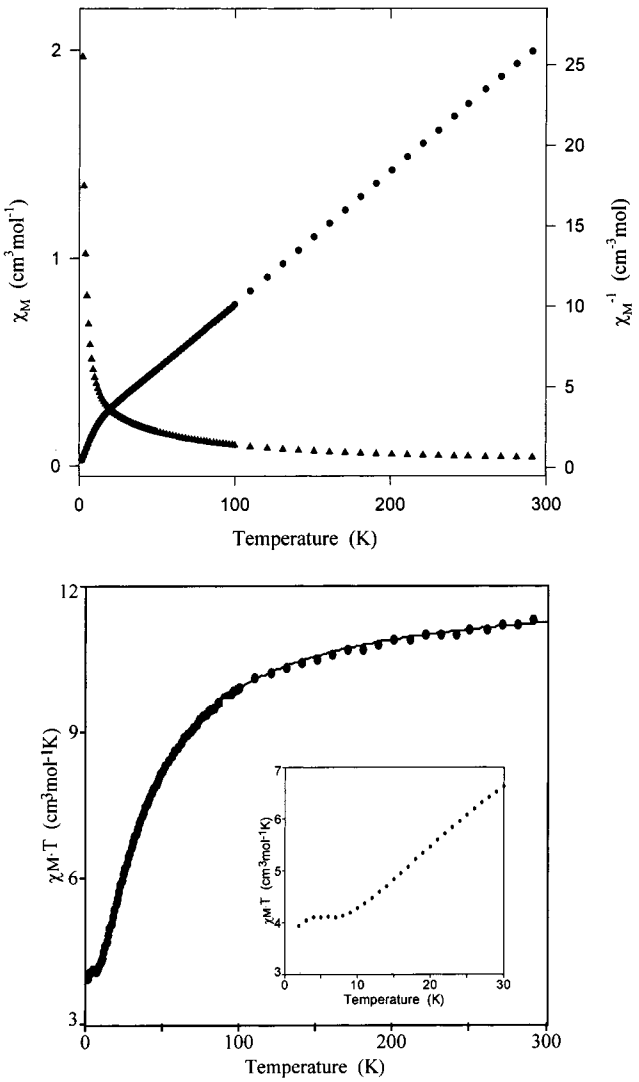

Figure 5. Temperature-dependent magnetic susceptibility data for **1**: (top) χ_M vs T (▲) and χ_M^{-1} vs T (●) plots; (bottom) $\chi_M T$ vs T plot.

structures, e.g., $Mn_3(OH)_2[B(OH)_4(PO_4)_4$[23] and $KMn_4(PO_4)_3$.[24] In both cases, the clusters connect to infinite chains and are not in discrete forms. Compound **1** is believed to be the first 3-D framework encapsulating linear trinuclear Mn−O clusters. Furthermore, the Mn(2) ion has four coordinated H_2O, two bridging with the Mn(1) ions and two being terminal ligands. Such a highly hydrated Mn^{II} compound is rare in metal phosphates except some natural minerals.[25] The title compound as well represents the first synthetic solid-state material containing the $Mn(H_2O)_4^{2+}$ cores. In addition to manganese, the other $M(H_2O)_4^{2+}$ cores in 3-D transition metal phosphates are found to exist in the hydrothermally synthesized $M_{0.5}VOPO_4{\cdot}2H_2O$ compounds with M = Co [26] and Ni.[27]

The linear $Mn_3(H_2O)_6O_8$ clusters reside inside the tunnels built from GaO_5 trigonal bipyramids and PO_4 tetrahedra. As shown in Figures 3, the three-dimensional GaPO framework can be viewed as built of porous $GaPO_4$ layers (Figure 3) of $Ga(1)O_5$, $Ga(2)O_5$, $P(1)O_4$, and $P(2)O_4$, joined by $P(3)O_4$ tetrahedra. It possesses intersecting tunnels respectively running along the [100] (Figure 3), [101], and [011] directions (Figure 4). The $Mn_3(H_2O)_6O_8$ clusters are delimited in the eight-ring tunnels primarily by sharing trans edges with two $P(3)O_4$ tetrahedra, resulting in the liner Mn_3P_2 pentamers lying on planes parallel to (001). In the interlayer region, as also shown in Figure 3, the Mn_3P_2 pentamers further connect to each other via hydrogen bonds formed between the terminal water hydrogen on O(15) and the phosphate oxygen O(12). The clusters also form H-bonds to the $GaPO_4$ layers, i.e., via the H-bonds between

(18) Sheldrick, G. M. *SADABS. Siemens Area Dector Absorption Correction Software;* University of Göttingen, Germany.
(19) Brown, I. D.; Altermann, D. *Acta Crystallogr.* **1985**, *B41*, 244.
(20) Sheldrick, G. M. *SHELXTL-Plus NT crystallographic system*, release 5.10; Bruker Analytical X-ray Systems: Madison, WI, 1998.
(21) Selwood, P. W. *Magnetochemistry*; Interscience: New York, 1956.
(22) (a) Rardin, R. L.; Bino, A.; Poganiuch, P.; Tolman, W. B.; Liu, S.; Lippard, S. J. *Angew. Chem., Int. Ed. Engl.* **1990**, *29*, 812. (b) Rardin, R. L.; Poganiuch, P.; Bino, A.; Goldberg, D. P.; Tolman, W. B.; Liu, S.; Lippard, S. J. *J. Am. Chem. Soc.* **1992**, *114*, 5240. (c) Tangoulis, V.; Malamatari, D. A.; Soulti, K.; Stergiou, V.; Raptopoulou, C. P.; Terzis, A.; Kabanos, T. A.; Kessissoglou, D. P. *Inorg. Chem.* **1996**, *35*, 4974.
(23) Moore, P. B.; Ghose, S. *Am. Mineral.* **1971**, *56*, 1527.
(24) Daidouh, A.; Martinez, J. L.; Pico, C.; Veiga, M. L. *J. Solid State Chem.* **1999**, *144*, 169.
(25) (a) Burns, P. C.; Hawthorne, F. C. *Am. Mineral.* **1995**, *80*, 620. (b) Kampf, A. R. *Am. Mineral.* **1977**, *62*, 250.
(26) Kang, H. Y.; Lee, W. C.; Wang, S. L.; Lii, K. H. *Inorg. Chem.* **1992**, *31*, 4743.
(27) Lii, K. H.; Wu, L. S.; Gau, H. M. *Inorg. Chem.* **1993**, *32*, 4153.

the terminal water hydrogen on O(13) and the phosphate oxygen atoms O(2) and O(4). Since the bond length of Mn−O(14) is the longest (thus the weakest) among all $Mn-O_{water}$ bonds, we propose that the two water molecules released at ca. 244 °C in the TGA/DTA curves (see Figure 1) should correspond to the bridging $H_2O(14)$ while the four water molecules released at ca. 334 °C should correspond to the H-bonded terminal water ligands $H_2O(13)$ and $H_2O(15)$. It is also noted that because of the edge-sharing with a $P(3)O_4$ tetrahedron and the lack of as many water ligands as Mn(2), the terminal $Mn(1)(H_2O)_2O_4$ exhibits much more octahedral distortion than the central $Mn(2)(H_2O)_4O_2$ ($10^4\Delta = 29.8$ vs 8.8).

The magnetic data, in the forms of χ_M vs T, χ_M^{-1} vs T, and $\chi_M T$ vs T plots are shown in Figure 5. As can be seen in the plot, the χ_M data between 300 and 50 K are described very well by a Curie−Weiss behavior: $\chi_M = C/(T - \theta)$, where $C = 12.15$ cm^3 K mol^{-1} is the Curie constant and $\theta = -23.5$ K is the Weiss temperature. There is no turn-down point in the χ_M vs T plot. However, the slow decrease of $\chi_M T$ with decreasing temperature is characteristic of an antiferromagnetic interaction, consistent with the negative sign of the Weiss temperature. At 300 K, the effective magnetic moment $\mu_{eff} = 9.52\mu_B$ per trimer ($5.49\mu_B$ per Mn^{II} center) is already much smaller than that of the spin-only value $10.25\mu_B$ per trimer ($5.92\mu_B$ per Mn^{II} center). The significant deviation of μ_{eff} may be caused by the spin−orbit coupling of Mn(II) in an equatorially distorted octahedral environment. Taking into account the isolated and linear form of $Mn_3(H_2O)_6O_8$ in **1** and assuming that the exchange coupling within the cluster is isotropic and that there is no interaction between two terminal Mn^{II} centers, the Heisenberg Hamiltonian for the $Mn_{(1)}Mn_{(2)}Mn_{(3)}$ system can be written as

$$H = -J[S_{(1)}S_{(2)} + S_{(2)}S_{(3)}]$$

where J is the exchange coupling constant (negative for an antiferromagnetic *AF* interaction, positive for a ferromagnetic *F* interaction) and $S_{(1)} = S_{(2)} = S_{(3)} = {}^5/_2$ for the three Mn^{II} centers in the system. By application of Van Vleck's equation,[28] the following theoretical expression for molar susceptibility may be derived:

$$\chi_M = \frac{Ng^2\beta^2}{3kT}\left(\frac{3F1}{4F2}\right) + \chi_{TIP} \qquad (1)$$

where

$$F1 = 680\,e^{27.5x} + 455(e^{20x} + e^{25x}) + 286(e^{13.5x} + e^{18.5x} + e^{22.5x}) + 165(e^{8x} + e^{13x} + e^{17x} + e^{20x}) + 84(e^{3.5x} + e^{8.5x} + e^{12.5x} + e^{15.5x} + e^{17.5x}) + 35(e^{15x} + e^{5x} + e^{9x} + e^{12x} + e^{14x}) + 10(e^{2.5x} + e^{6.5x} + e^{9.5x} + e^{11.5x}) + (e^{5x} + e^{8x}) + 35$$

$$F2 = 8\,e^{27.5x} + 7(e^{20x} + e^{25x}) + 6(e^{13.5x} + e^{18.5x} + e^{22.5x}) + 5(e^{8x} + e^{13x} + e^{17x} + e^{20x}) + 4(e^{3.5x} + e^{8.5x} + e^{12.5x} + e^{15.5x} + e^{17.5x}) + 3(e^{15x} + e^{5x} + e^{9x} + e^{12x} + e^{14x}) + 2(e^{2.5x} + e^{6.5x} + e^{9.5x} + e^{11.5x}) + (e^{5x} + e^{8x}) + 3$$

$x = J/(kT)$ and the χ_{TIP} term were added to take into account the temperature-independent paramagnetic contribution from the sample. A quantitative fit of eq 1 to the whole data was obtained for reasonable values of the adjustable parameters $J = -3.35$ cm^{-1}, $g = 1.91$, and $\chi_{TIP} = 1.8 \times 10^{-5}$ cm^3 mol^{-1} and is shown in Figure 5 (solid curve).

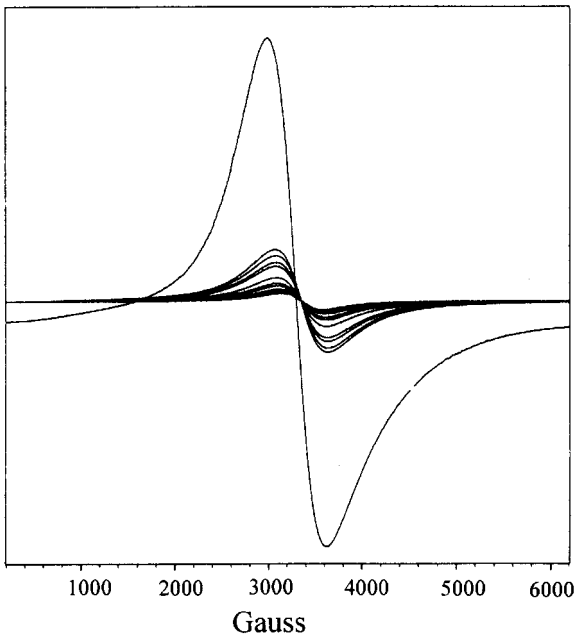

Figure 6. Powder X-band EPR spectra of **1** measured at 300, 200, 150, 100, 80, 50, 20, 15, 10, 8, and 6 K (in the order from the smallest to the largest signal).

It is interesting to note that $\chi_M T$ reaches the first minimum in the 8−4 K range at a constant value of 4.1 cm^3 K mol^{-1} (see the inset of Figure 5), which corresponds (within experimental uncertainty) to the expected value $\chi_M T = Ng^2\beta^2S(S + 1)/(3k)$ for a spin $S = {}^5/_2$ state with $g = 2$. The Curie behavior at such low temperatures has not been observed in the existing $Mn^{II}Mn^{II}Mn^{II}$ molecular complexes that have been studied until now.[22] To further confirm the presence of a free spin in the system, the measurements of EPR spectra at various temperatures were performed on the title compound. In Figure 6, the temperature-dependent intensities clearly show Curie variation of the signal. The sharp maximum at 6 K confirms the existence of an isolated spin of Mn^{II}. A vivid way to describe the Curie behavior of **1** is to say that the two ${}^5/_2$ local spins on the terminal Mn^{II} centers are aligned along a common direction through the antiferromagnetic interaction with the ${}^5/_2$ spin of the central Mn^{II} center. In some way, one of the two terminal spins and the central spin cancel out completely, resulting in a paramagnetic-like fashion. Since the $Mn_3(H_2O)O_8$ clusters lying in the same tunnel can be as close as 6.04 Å, intercluster interactions should emerge at lower temperatures. Indeed, when the sample is cooled, the $\chi_M T$ slightly decreases with temperature below 4 K, where a 3-D antiferromagnetic ordered structure might be attained.

In conclusion, a novel nonorganically templated manganese gallium phosphate has been synthesized and characterized. The GaPO open framework contains three-dimensional intersecting tunnels in which unusual $Mn_3(H_2O)_6$ cores are encapsulated via Mn−O−Ga(or P) bonds. In contrast to all existing transition-metal-substituted gallium phosphates where the transition metals occupy framework sites, the manganese ions cluster together and fill the space that used to be occupied by organic templates. At high temperatures, the antiferromagnetic behavior of the $Mn_3(H_2O)_6$ core in the current GaPO lattice is similar to that of trimanganese molecular complexes.[22] But at low temperatures, magnetic coupling of the $Mn_3(H_2O)_6$ cores gives rise to a

(28) Kahn, O. *Molecular Magnetism*; VCH Publishers, Inc.: New York, 1993; p 211.

pronounced Curie behavior not observed in molecular $Mn3^{II}$ structures before.

Acknowledgment. We thank the National Science Council and Chinese Petroleum Corp. of Taiwan for support of this work (NSC 89-2113-M-007 -025 and NSC 87-CPC -M-007 -001). We are also grateful to Professor K. H. Lii for valuable discussions and help with the magnetic study.

Supporting Information Available: X-ray crystallographic data including tables of complete crystal data, atomic coordinates, bond distances and angles, and anisotropic thermal parameters for **1**. This material is available free of charge via the Internet at http://pubs.acs.org.

IC991340S